IEEE Access
Multidisciplinary | Rapid Review | Open Access Journal

Received 13 July 2022, accepted 5 August 2022, date of publication 18 August 2022, date of current version 24 August 2022.

Digital Object Identifier 10.1109/ACCESS.2022.3199925

METHODS

Battery Current-Sharing Power Decoupling Method for Realizing a Single-Stage Hybrid PV System

LIANG-RUI CHEN[1], (Member, IEEE), CHIA-HSUAN WU[2], NENG-YI CHU[3], CHENG-CHIH CHOU[1,4], AND FAN-JUN ZHENG[5]

[1]Department of Electrical Engineering, National Changhua University of Education, Changhua 50074, Taiwan
[2]Department of Industrial Education and Technology, National Changhua University of Education, Changhua 50074, Taiwan
[3]Department of Electrical Engineering, National Penghu University of Science and Technology, Penghu 880011, Taiwan
[4]Green Energy and Environment Research Laboratories, Industrial Technology Research Institute, Hsinchu 31057, Taiwan
[5]P-DUKE Technology Company Ltd., Taichung 40850, Taiwan

Corresponding author: Chia-Hsuan Wu (swdemperor@hotmail.com)

ABSTRACT Conventionally, the single-stage grid-connected PV inverter needs a large PV-side electrolytic capacitor to suppress the double-line frequency current ripple to keep the PV operating at maximum power point (MPP). However, the short lifetime electrolytic capacitor will reduce the PV inverter's reliability dramatically. In order to overcome the above problem, a novel battery current-sharing power decoupling (BCSPD) method for hybrid photovoltaic (PV) power systems is proposed in this paper. The proposed BCSPD circuit is parallelly connected with the string PV module to achieve as a single-stage topology. Thus, a high power conversation efficiency can be obtained. The current-injection method is adapted to solve the current ripple problem. Therefore, the required capacitance in PV side can be greatly reduced, so long-life film capacitors can be used instead of electrolytic capacitors. In addition, the battery storage system with the droop control is also used to realize the power regulation function to meet the requirements of actual applications. A 1200 W prototype was designed and implemented to assess the system performance. Experimental results show that the proposed system can track MPP, regulate the load power condition, and reduce current ripple.

INDEX TERMS Current-shared, maximum power point tracking, photovoltaic power system.

I. INTRODUCTION

In recent years, the grid-connected photovoltaic (PV) power system has been developed dramatically and gradually to form a considerable part of the main grid because the environmental concern and continuous depletion of fossil fuel reserves. Conventionally, string of PV modules is serially connected to a high enough voltage and connected to a PV inverter (i.e., a grid-connected PV inverter). The traditional PV inverter is divided into single-stage and two-stage [1], [2], [3], [4], [5]. The single-stage PV inverter has a high power conversion efficiency as shown in Figure 1. Unfortunately, the single-stage PV inverter has a double-line-frequency current ripple in the PV side [6], [7]. In order to briefly describe the double-line-frequency current ripple phenomenon, assume that the grid voltage $v_O(t)$ and the injected current $i_O(t)$ are given as (1) and (2).

$$v_O(t) = V_m \cos(\omega_0 t) \tag{1}$$

$$i_O(t) = I \cos(\omega_0 t) \tag{2}$$

where ω_0 is the line frequency, V_m is the line peak voltage, and I is the injected peak current. The instantaneous output power p_O(t) can be shown as (3).

$$p_O(\mathrm{t}) = v_O(t) \times i_O(t) = \frac{1}{2} V_m I + \frac{1}{2} V_m I \cos(2\omega_0 t) \tag{3}$$

By ignoring the losses in the inverter, the power generated by the PV panel will be equal to the output power p_O(t).

The associate editor coordinating the review of this manuscript and approving it for publication was Giambattista Gruosso.

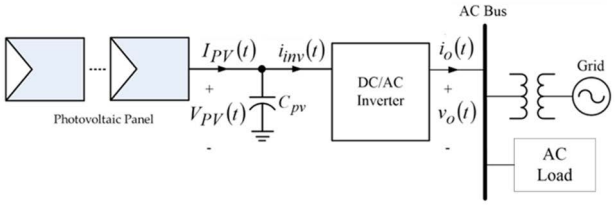

FIGURE 1. The single-state PV inverter.

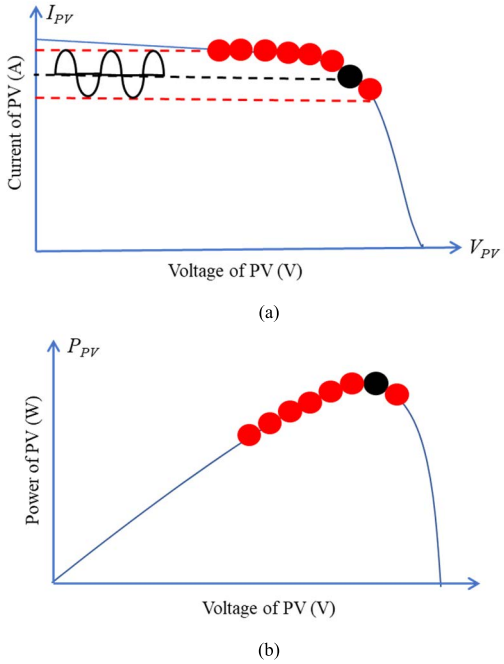

FIGURE 2. The effect of ripple current on (a) VI curve and (b) VP curve.

This means that there is a significant and huge double-line-frequency ripple current in the PV panel. Therefore, the operating point cannot be maintained at the maximum power point (MPP) as shown in Figure 2. This results in a significant reduction in PV panel output power.

A usual solution to reduce the double-line-frequency current ripple is to use a large electrolytic capacitor (i.e., decoupling capacitor C_{pv} as shown in Figure 1) at the DC link to buffer the ripple power. However, the short lifetime electrolytic capacitor will reduce the PV inverter's reliability dramatically, and weight and volume are obviously increased. Thus, the two-stage topology, as shown in Figure 3, was used to avoid the current ripple problem at the PV side [8], [9], [10]. However, the cost, weight, volume and efficiency of a two-stage topology are worse than that of a single-stage topology. Furthermore, the typical two-stage topology cannot comply with the European standards EN50160, which stipulate that the low frequency voltage pulsation of the DC bus voltage should be kept within the range of 2%.

In the other method, active decoupling circuits connected at the PV side or AC side were proposed to sink the ripple current [8], [11], [12], [13], [14], [15]. This kind of active

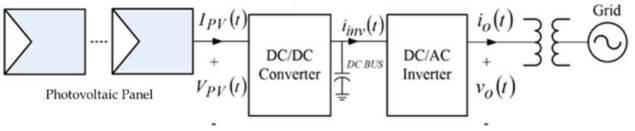

FIGURE 3. The two-stage PV power system.

power decoupling techniques utilize auxiliary power electronic circuits to pump/sink the ripple power into small film capacitors which can be used to replace the large electrolytic capacitor. Although active power decoupling techniques can effectively suppress the ripple current, they increase circuit complexity and cost.

In reality, sunlight is not constant, and the loads and PV power are often mismatched. When much more energy being is produced in the PVs than is being consumed by the loads, the grid will be fluctuated [16]. The droop control PV inverter was used to overcome this problem [17], [18]. However, generated energy of the PV modules is wasted. Therefore, a hybrid PV power system (i.e., grid-connected PV inverter with battery storage system), shown as Figure 4, was suggested to store the extra power in the battery and then smoothly inject power to the grid to solve this problem [19], [20]. Battery storage systems assist in performing one or more important tasks such as (i) smoothing power fluctuation [21], [22], (ii) shift peak generation period, and (iii) protection during outages when installed along with large PV generation.

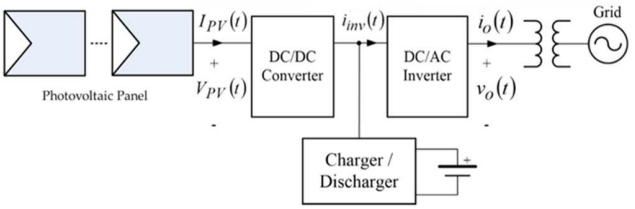

FIGURE 4. The hybrid PV power system.

In this paper, an active decoupling function tries to be realized by using a battery storage system, then the DC/DC converter in a conventional hybrid PV power system can be eliminated. Thus, a hybrid PV power system with single-stage topology can be realized to reduce the power conversion loss. In addition, the battery storage system with the droop control is used to realize the power regulation functions. Experimental results show that the proposed method can really track the MPP of the PV modules, regulate the load power, reduce the current ripple, and reduce the circuit components and cost as we wanted.

II. SYSTEM DESCRIPTION

The presented battery current-sharing power decoupling (BCSPD) circuit is mainly constructed by a bidirectional dc/dc converter and parallel-connected with the PV modules and the PV inverter, as shown in Figure 5. Compared with the traditional hybrid PV power system as shown in Figure 4,

We can see that the DC/DC converter can be eliminated and there is only a single power stage between PV modules and load in the proposed system. So, the single-stage hybrid PV power system is achieved by using the proposed methods. The presented BCSPD circuit is composed of an input capacitor C_i, two power MOSFETs S_1 and S_2, an inductor L and an output capacitor C_o. Diodes D_1 and D_2 are the body diodes of power MOSFETs S_1 and S_2.

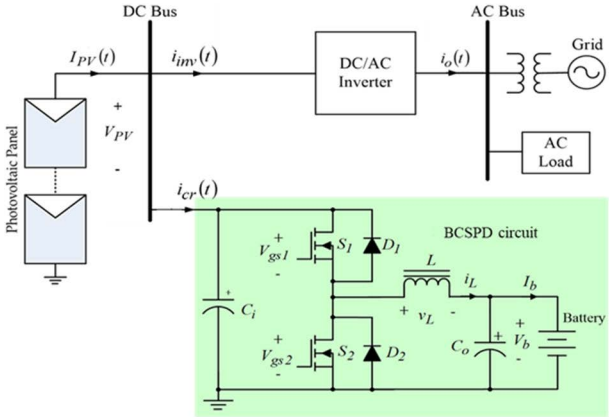

FIGURE 5. The block diagram of the proposed BCSPD circuit for PV power applications.

Figure 6 shows the waveforms of the proposed BCSPD circuit. Note that the gate-source voltages V_{gs1} and V_{gs2} are complementary and circuit works like a synchronous switching buck/boost converter. The duty cycle of the inductor voltage is controlled by the gate-source voltages V_{gs1} and V_{gs2}. The inductor current of the bidirectional dc/dc converter i_L can be written as (4) according to Volt-Second balance law.

$$i_L = \frac{V_{PV}D - V_b}{L \cdot f_s} \tag{4}$$

where

V_{PV} is the voltage of the PV modules,

D is the PWM duty ratio of the bidirectional dc/dc converter,

V_b is the average battery voltage (V),

f_s is the switch frequency (Hz), and

L is the inductance (H).

The regulation current i_{cr} is the input current of the proposed BCSPD circuit. According to a typical buck converter theory, the input current is the D times of the inductor current. Thus, the regulation current i_{cr} can be defined as

$$i_{cr} = i_L \cdot D = \frac{V_{PV}D - V_b}{L \cdot f_s} \cdot D \tag{5}$$

From (5), we can know that the regulation current i_{cr} is positive to charge battery

When D> (V_b/V_{PV}). Oppositely, the regulation current i_{cr} is negative to discharge battery

when D< (V_b/V_{PV}).

From (2), the proposed BCSPD circuit can be viewed as controllable current source. The dc/ac inverter with load can

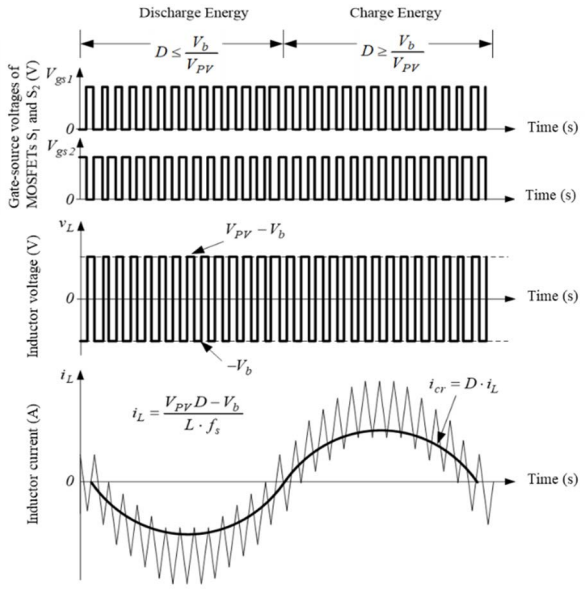

FIGURE 6. The waveforms of the proposed BCSPD circuit.

be view as a variable current load and shown as

$$i_{inv}(t) = \frac{v_{o,rms} \cdot i_{o,rms} \cdot (1 - cos\, 2\omega t)}{V_{PV}} \tag{6}$$

where

V_{PV} is the PV module output voltage (V),

$v_{o,rms}$ is the rms values of the AC bus voltage (V),

$i_{o,rms}$ is the rms values of the inverter injecting current (A), and

ω is the grid frequency.

Thus, the simplified model can be plotted as Figure 7. In which, the model of PV module equals a PN junction semiconductor when sunlight can produce a current source I_{PV}.

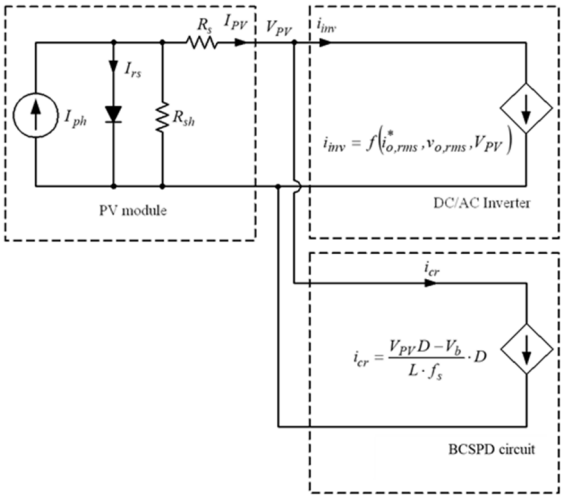

FIGURE 7. The simplified model of the proposed BCSPD circuit for PV power applications.

Figure 8 shows the flowchart of the proposed system. First, the root-mean-square (rms) of the grid voltage $v_{o,rms}$ is measured. Then the rms value of the injecting current $i_{o,rms}$ can be decided by the droop control method to realize the power regulation.

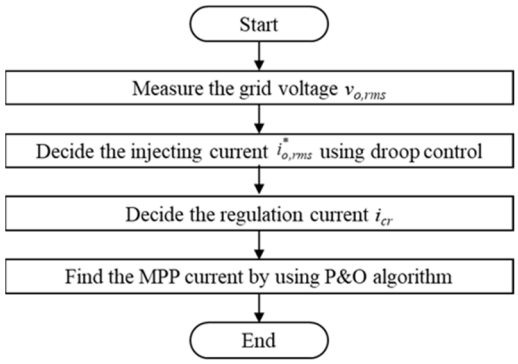

FIGURE 8. The flowchart of the proposed system.

Figure 9 shows the drop control diagram for the injecting current $i^*_{o,rms}$. If the grid voltage $v_{o,rms}$ is larger than the standard utility voltage $v_{utility}$, the injecting current $i^*_{o,rms}$ should be negative to release power from battery to the grid to increase the grid voltage. And the injecting current $i^*_{o,rms}$ becomes larger as the voltage error $v_{o,rms} - v_{utility}$ increases. If the grid voltage $v_{o,rms}$ is smaller than the standard utility voltage $v_{utility}$, the injecting current $i^*_{o,rms}$ should be positive to absorb power from grid to the battery, thus reducing the grid voltage.

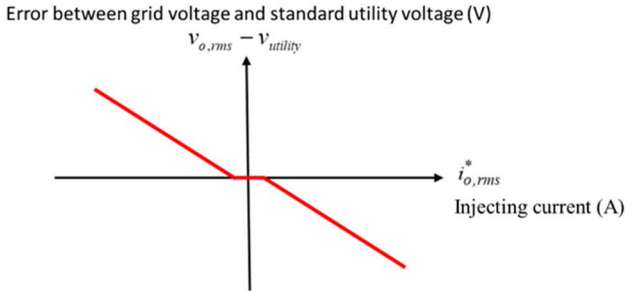

FIGURE 9. The drop control diagram for the injecting current $i^*_{o,rms}$.

After that, the perturbation and observation (P&O) algorithm is used to find I^*_{PV}. According to Figure 7 and Kirchhoff's current laws, the output current of the PV modules I_{PV} is the sum of the input current of the PV inverter i_{inv} and the regulation current of the proposed BCSPD circuit i_{cr}. Thus, to achieve works of the PV modules in the MPP and to regulate PREETHI the PV inverter power, the regulation current of the proposed BCSPD circuit i_{cr} can be decided by

$$\begin{aligned} i_{cr}(t) &= I^*_{PV} - i_{inv}(t) \\ &= I^*_{PV} - \frac{v_{o,rms} \cdot i^*_{o,rms}(1 - \cos 2\omega t)}{V_{PV}} \end{aligned} \tag{7}$$

Figure 10 is the system operation waveform diagram. When the input current of the PV inverter $i_{inv}(t)$ is smaller than the MPP current of the PV modules I^*_{PV}. The proposed BCSPD circuit will charge a completely complementary current. It reduces the PV modules current ripple and achieves the PV modules MPPT control. As shown in Figure 10, the gray area is the charge energy in the battery. When the input current of the PV inverter $i_{inv}(t)$ is larger than the MPP current of the PV modules I^*_{PV}. The proposed BCSPD circuit can generate a completely complementary ripple current to reduce the PV modules current ripple, as shown in Figure 10. The black area is the discharge energy. The proposed CS-MPPT with ripple reducing system can reduce the variable value of the injected power to improve the power quality of the grid. In addition, it can reduce the PV modules current ripple to increase the PV output power.

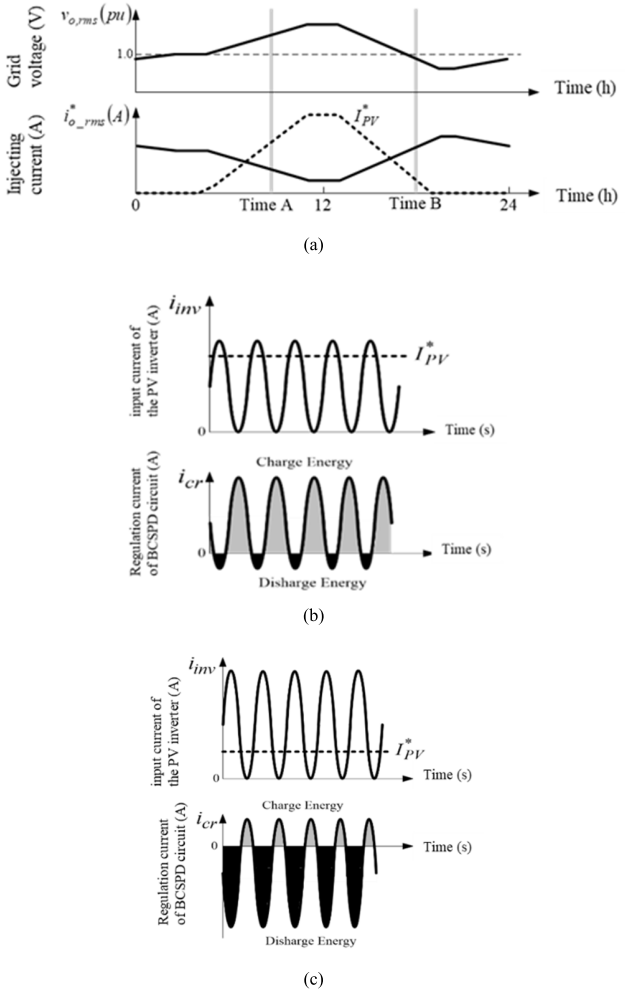

FIGURE 10. System operation timing diagram (a) duration a day (b) at Time A and (c) at Time B.

III. DESIGN CONSIDERATION

There are two kinds of current ripple influence the MPPT. One is the PWM switching current ripple (i.e., high frequency current ripple) from the BCSPD circuit, the other is the twice

utility frequency current ripple (i.e., low frequency current ripple). In order to reduce the high frequency current ripple, the input capacitor C_i is used, and its value can be decided by

$$C_i \geq \frac{I_{cr,\max}}{2 \cdot V_{PV} \cdot r \cdot f} \tag{8}$$

where r is the ripple factor.

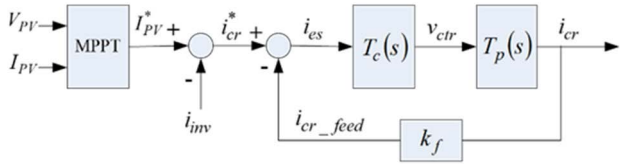

FIGURE 11. The control loop.

In order to ensure that the proposed BCSPD circuit can provide the required compensation current of the low frequency current ripple, the small signal analysis is used to check the system control loop stability and frequency response. Figure 11 is the control loop of the proposed system. In which, the $T_p(s)$, $T_c(s)$, and k_f are the transfer functions of the bidirectional converter, the compensation circuit and the feedback gain. The transfer function $T_p(s)$ can be written as

$$T_p(s) = \left.\frac{\tilde{i}_{cr}(s)}{\tilde{v}_{ctr}(s)}\right|_{\tilde{v}_b(s)=0} = \frac{1}{V_r} \times \frac{sLI_b + V_b}{r_s LC_i\left(s^2 + \frac{1}{r_s C_i}s + \frac{D^2}{LC_i}\right)} \tag{9}$$

where

$\tilde{v}_b$ is the small signal of the battery voltage (V),
V_r is the serrated waveform with amplitude (V),
I_b is the average battery current (A),
r_s is the internal resistance of the battery (Ω), and
C_i is the input capacitance of the bidirectional DC/DC converter (F).

$$\text{Zero}: f_{Tp\_z} = \frac{V_b}{2\pi LI_b} \tag{10}$$

$$\text{Pole}: f_{Tp\_p1} = \frac{\left(\frac{1}{r_s C_i} - \sqrt{\left(\frac{1}{r_s C_i}\right)^2 - \frac{4D^2}{LC_i}}\right)}{4\pi} \tag{11}$$

$$f_{Tp\_p2} = \frac{\left(\frac{1}{r_s C_i} + \sqrt{\left(\frac{1}{r_s C_i}\right)^2 - \frac{4D^2}{LC_i}}\right)}{4\pi} \tag{12}$$

According to (10)–(12), the bode plot of the open loop transfer function can be drawn clearly, as shown in Figure 12. Obviously, there is a phase shift P_r at the ripple current frequency $f_r = 2f_{ac}$. In order to reduce the phase shift to zero, the lead compensation circuit as shown in Figure 13 is used. In order to simplify the mathematical formulas and circuit diagrams, resistors and capacitors with the same resistance value or the same capacitance value are represented by the same component numbers. The transfer function of the lead

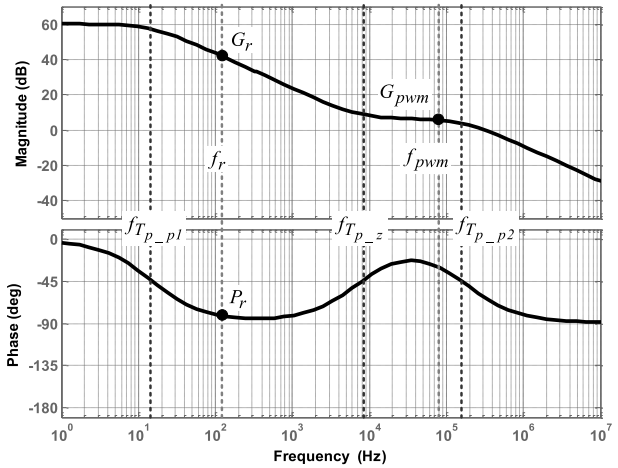

FIGURE 12. The bode plot of $T_p(s)$.

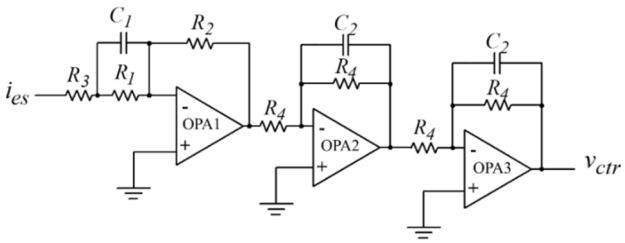

FIGURE 13. The lead compensation circuit.

compensation circuit can be defined as (13). In Figure 13, resistors R_1, R_2, R_3, capacitor C_1, and operational amplifier OPA1 create a zero frequency, as shown in Equation (14), and a pole frequency as shown in Equation (15), and its gain is shown in Equation (17). The resistor R_4 and capacitor C_2 and operational amplifiers OPA2 and OPA3 create a pole frequency as shown in Equation (16).

$$T_c(s) = \left(\frac{R_2}{R_1 + R_2}\right) \cdot \frac{1 + SR_1C_1}{\left(1 + S\frac{R_1R_2C_1}{R_1+R_2}\right) \cdot (1 + SR_4C_2) \cdot (1 + SR_4C_2)} \tag{13}$$

The zeros, poles and gain of the lead compensation circuit can be expressed as

$$\text{Zero}: f_{T_{c\_z}} = \frac{1}{2\pi C_1 R_1} \tag{14}$$

$$\text{Pole } f_{T_{c\_p1}} = \frac{1}{2\pi \frac{C_1R_1R_3}{R_3+R_1}} \tag{15}$$

$$f_{T_{c\_p2}} = \frac{1}{2\pi C_2 R_4} \tag{16}$$

$$\text{Gain}: k_{T_c} = \frac{R_2}{R_1 + R_3} \tag{17}$$

The compensation criteria are listed as following:

1. The gain margin and the phase margin should be large than 20dB and 45° to ensure the proposed system being stable.
2. The bandwidth should be larger than $10f_r$ to ensure the proposed system tracking the input current of the PV inverter.
3. The gain at switching frequency f_{pwm} should be smaller than −20dB to ensure the switching noise being small enough.
4. The phase shift P_r of the ripple current frequency should be close to zero to reduce the phase shift error at frequency f_r.
5. To meet these compensation criteria, the frequencies of the zero and poles in the lead compensation circuit can be set as:

$$f_{Tc\_z} = f_{Tp\_p1}, \tag{18}$$
$$f_{Tc\_p1} = f_{Tp\_z}, \text{ and} \tag{19}$$
$$f_{Tc\_p2} = f_{Tp\_p2} \tag{20}$$

In battery storage systems, there are many battery charging strategies which can be selected. In this design example, the general variable current charging strategy is used to minimize the control complexity.

IV. DESIGN EXAMPLE

In this section, the proposed BCSPD circuit prototype was developed to apply in a 1200 W PV system. Table 1 is the electrical specifications of the proposed system prototype. The circuit diagram of the BCSPD circuit prototype is shown in Figure 14. It was mainly constructed by a bidirectional DC/DC converter. The main components and parameters in the design example are listed in Table 2. A Microcontroller HT66F50 and operational amplifier (OP Amp) TL084 are used as the control unit. Note that a 1200w PV system without the proposed BCSPD method, an 8mF capacitor is needed [7] to filter the 120Hz current ripple. By the proposed BCSPD method, the large capacitor can be removed, only a 10uF capacitor is needed.

TABLE 1. Electrical specifications of the proposed system.

System Power P_o	1200 W
The MPP voltage of PV modules V_{PV}	150 V
The maximum regulation current i_{cr}(t)	±8 A
Battery voltage V_b	48 V
Grid frequency f_{ac}	60 Hz
Ripple current frequency f_r	120 Hz

According to (14)–(17) and the component parameter in Table 2, frequencies of the zero and poles in the lead compensation circuit are

$$f_{Tc\_z} = f_{Tp\_p1} = 15 \text{ Hz}, \tag{21}$$
$$f_{Tc\_p1} = f_{Tp\_z} = 7.34 \text{ kHz} \tag{22}$$
$$f_{Tc\_p2} = f_{Tp\_p2} = 172.98 \text{ kHz}. \tag{23}$$

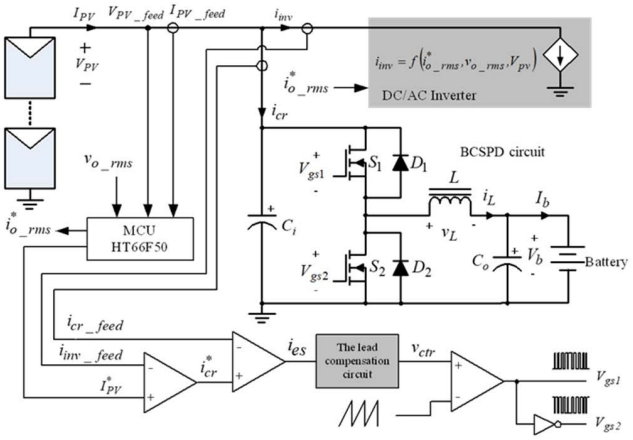

FIGURE 14. The configuration of the proposed BCSPD circuit.

TABLE 2. Main components and parameters.

Power MOSFETs S_1 and S_2	IRF460
Microcontroller	HT66F50
OP Amp	TL084
Filter inductance L	100 μH
Input capacitance C_i	10 μF
Output capacitance C_o	100 μF
Switch frequency f_{pwm}	80 kHz
Compensation resistance R_1	106 kΩ
Compensation resistance R_2	10.6 MΩ
Compensation resistance R_3	217 Ω
Compensation resistance R_4	1.3 kΩ
Compensation capacitance C_1	0.1 μF
Compensation capacitance C_2	0.01 μF

Thus, $R_1 = 106\text{k}\ \Omega$, $R_2 = 10.6\text{M}\ \Omega$, $R_3 = 217\ \Omega$, $R_4 = 1.3\text{k}\ \Omega$, $C_1 = 0.1\ \mu\text{F}$, $C_2 = 0.01\ \mu\text{F}$ are used in the compensation circuit. In order to reduce the PWM switching ripple current, (8) with ripple factor $r = 0.03$ is used. The input capacitor C_i can be obtained as 10 μF.

V. EXPERIMENTS

A 1200 W BCSPD circuit prototype was realized and shown as Figure 15 to assess system performance. Table 3 shows the used solar panel parameters. The experiment PV array was constructed by five solar panels connected in series.

TABLE 3. The solar panel parameters.

Maximum power	230 W
MPP voltage @1000 W/m2, 25 °C	30 V
MPP current @1000 W/m2, 25 °C	7 A
Module efficiency	13.4%
Solar cell efficiency	16.4%

Figure 16 is the bode plot of the close loop transfer function. From Figure 16, we can find that the gain margin, the phase margin and the bandwidth of the realized system are 23.6 dB, 81.4°, and 7.41 kHz. In addition, the gain and phase shift of the realized system at the ripple current frequency f_r are 6.72 dB and −1.33°, respectively. Figure 17 shows

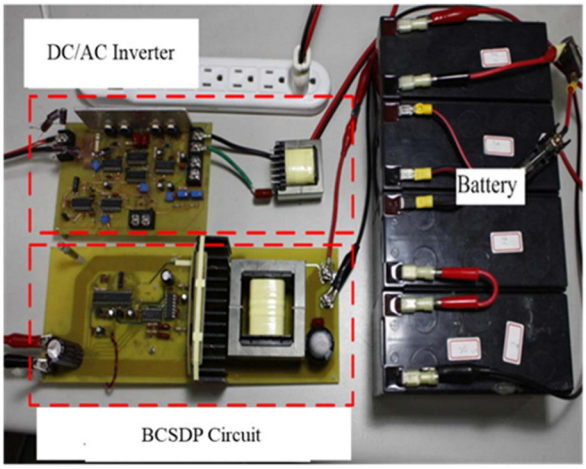

FIGURE 15. The realized 1200 W BCSPD circuit prototype.

the regulation current control signal i_{cr}^{*} and the regulation current i_{cr} with and without compensation. It is clear that the proposed BCSPD circuit can generate a completely complementary ripple current to reduce the PV modules current ripple as we wanted.

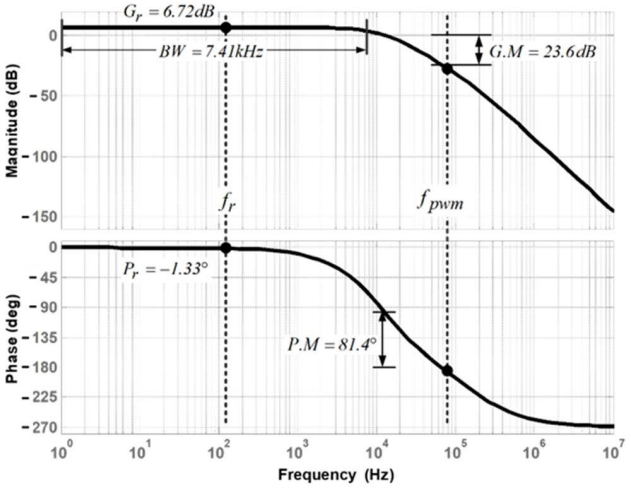

FIGURE 16. The close loop bode plot of the prototype.

In order to measure the voltage and current waveform, a digital 4-channel oscilloscope and three current probes are used. Figure 18 shows experiment waveforms of the PV power system without the current ripple reducing function. Clearly, the PV modules has a current ripple that is caused by the DC/AC inverter. The output ripple current of the PV modules ΔI_{PV} is 10A and the output ripple voltage of the PV modules ΔV_{PV} is 70 V. Therefore, the output power of PV modules is the time-variable value. The operation point of the PV modules does not operate at MPP. Figure 19 shows experiment waveforms of the proposed BCSPD circuit. We can see that the proposed BCSPD circuit can generate a completely complementary current ripple to

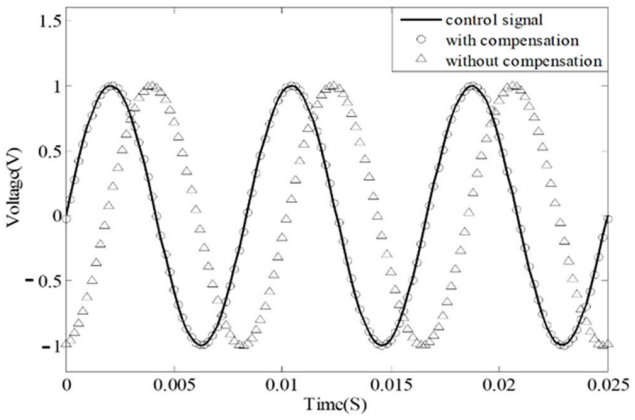

FIGURE 17. The regulation current control signal i_{cr}^{*} and the regulation current i_{cr} with and without compensation.

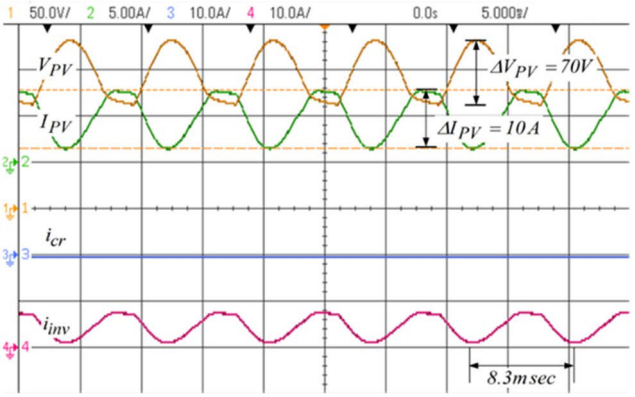

FIGURE 18. Experiment waveforms of the PV power system without the proposed BCSPD circuit.

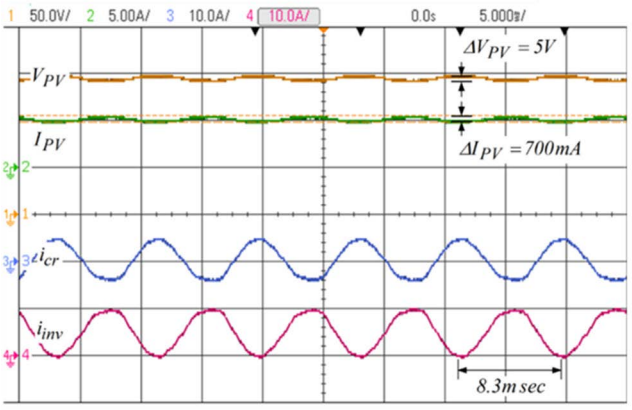

FIGURE 19. Experiment waveforms of the proposed BCSPD circuit.

reduce the PV modules current ripple from 10 A to 700 mA and the PV modules voltage ripple from 70 V to 5 V, obviously. The ripple current of the PV modules reduces to 3% and then the output power of the PV modules is increased.

Figure 20 shows the measured waveforms when the prototype works in daytime. Clearly, the average current of the DC/AC inverter i_{inv} (i.e., 1 A) is smaller than the current of the MPP I_{PV} (i.e., 5 A). We can see that the proposed BCSPD circuit works as charger with 4 A. to make the PV modules work at MPP and the current ripple reducing is also maintained. Figure 21 shows the measured waveforms when the prototype work at night. The current of the MPP I_{PV} is 0 A and the BCSPD circuit works as discharger with -3.5 A to make sure the utility power stability and the current ripple reducing is also maintained.

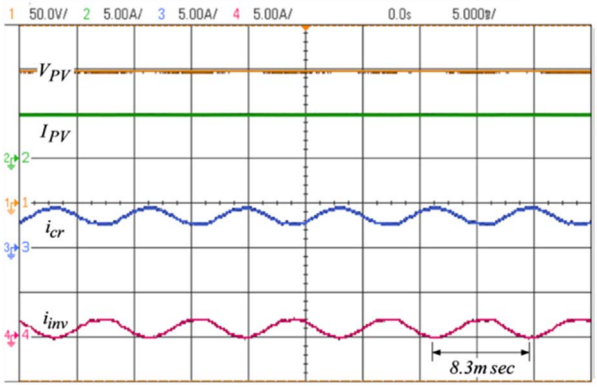

FIGURE 20. The measured waveforms when the proposed BCSPD circuit works in daytime.

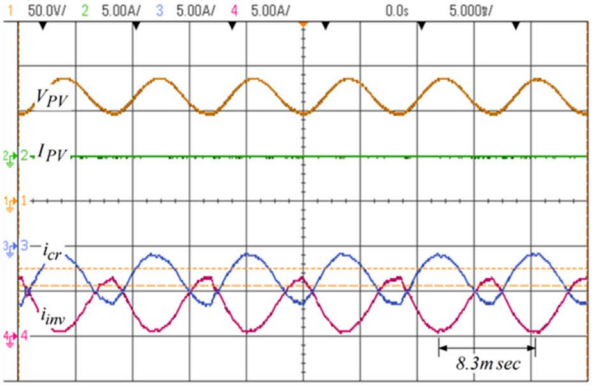

FIGURE 21. The measured waveforms when the proposed BCSPD circuit work at night.

In order to measure the MPPT performance, a recorder is used to measure and recode the PV operating voltage and PV operating current. Figure 22 shows the MPPT experiment results during the solar panel temperature is about 25 °C and the solar irradiance is varied in 700 W/m^2–800 W/m^2 range. The grey lines are the V-P curves of the used PV panel at solar irradiance = 700 W/m^2 and solar irradiance = 700 W/m^2, respectively. The black spots are the measured operating points of PV. Note that operating points of PV swings because of the solar irradiance are continuously varied. Clearly, the MPP is tracked from oscillating by the proposed system. This means that the double-line-frequency ripple current is eliminated, and maximum output power of the PV system is obtained.

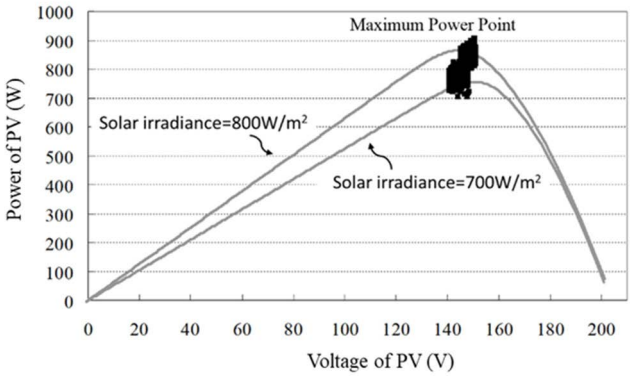

FIGURE 22. The 1200 W BCSPD circuit experiment result under solar irradiance is varied in 700 W/m^2–800 W/m^2 range.

VI. CONCLUSION

A traditional PV inverter is divided into single-stage and two-stage. Although the single-stage PV inverter has high power conversion efficiency, it has the problem of low-frequency ripple in PV. This causes a decrease in the efficiency of PV power generation. The two-stage PV inverter can be buffered by a DC bus without the problem of low-frequency ripple. Therefore, the efficiency of PV power generation is high. However, the two-stage PV inverter has one more series-connected DC/DC converter than the single-stage PV inverter, so the power conversion efficiency is low. In order to overcome the above problem, a novel CS-MPPT with ripple-reducing technology for PV power applications was successfully proposed in this paper. The proposed system is a parallel-connected structure, so its power conversion efficiency is as high as that of a single-stage PV inverter. In addition, the proposed CS-MPPT can track the MPP, regulate the load power condition and reduce current ripple at the same time. Therefore, a high efficiency of PV power generation is also obtained. In order to assess the proposed system performance, a 1200 W prototype was designed and implemented. Experiment results show that the proposed CS-MPPT with ripple reducing system can generate a completely complementary current ripple to reduce the PV modules current ripple from 10 A to 700 mA and the PV modules voltage ripple from 70 V to 5 V, obviously. Thus, the power efficiency of the PV modules is increased as theorical prediction. The feasibility and excellent performance of the proposed CS-MPPT with ripple reducing system are verified by experiment results.

A novel BCSPD technology for PV power applications was successfully proposed in this paper. The proposed system is a parallel-connected structure, so its power conversion efficiency is as high as that of a single-stage PV inverter. In addition, the proposed CS-MPPT can track the MPP, regulate the load power condition and reduce current ripple at the same time. Therefore, a high output power of PV power generation is also obtained. In order to assess the proposed system performance, a 1200 W prototype was

designed and implemented. Experiment results show that the proposed BCSPD circuit can generate a completely complementary current ripple to reduce the PV modules current ripple from 10 A to 700 mA and the PV modules voltage ripple from 70 V to 5 V, obviously. Thus, the output power of the PV modules is increased as theoretical prediction. The feasibility and excellent performance of the proposed BCSPD circuit are verified by experiment results.

APPENDIX- LIST OF FIGURE SYMBOL

NOMENCLATURE

V_{PV}	The voltage of the PV modules, V.
C_{pv}	The capacitance at the PV-side, F.
I_{PV}	The current of the PV modules, A.
I_{inv}	The input current of the inverter, A.
i_o	The output current of the inverter, A.
v_o	The output voltage of the inverter, V
i_{cr}	The regulation current of CS-MPPT, A.
i_{es}	The error current between the feedback current and the desired current, A.
v_L	The voltage of the inductor, V.
i_L	The current of inductor, A.
V_b	The average battery voltage, V.
V_{gs}	The gate-source voltage of MOSFET, V.
I_b	The average battery current, A.
C_i	The input capacitance of the bidirectional DC/DC converter, F.
C_o	The output capacitance of the bidirectional DC/DC converter, F.
f_s	The switch frequency, Hz.
$i_{o,rms}$	The rms values of the inverter injecting current, A.
$v_{o,rms}$	The rms values of the AC bus voltage, V.
I_{ph}	The light-generated current in the PV cell, A.
I_{rs}	The voltage-dependent current lost to recombination, A.
R_{sh}	The shunt resistance of the PV cell, R.
R_s	The series resistance of the PV cell, R.
T_c(s)	The transfer function of the compensation circuit.
T_p(s)	The transfer function of the bidirectional converter.
k_f	The feedback gain.
v_{ctr}	The control voltage.

ACRONYMS AND SUBSCRIPTS

DC	Direct Current.
AC	Alternating Current.
S	MOSFET.
D	The PWM duty ratio of the bidirectional dc/dc converter.
OPA	Operational Amplifier.
R	Resistance
L	Inductance

REFERENCES

[1] I. Vairavasundaram, V. Varadarajan, P. J. Pavankumar, R. K. Kanagavel, L. Ravi, and S. Vairavasundaram, "A review on small power rating PV inverter topologies and smart PV inverters," *Electronics*, vol. 10, no. 11, p. 1296, May 2021.

[2] M. N. H. Khan, M. Forouzesh, Y. P. Siwakoti, L. Li, T. Kerekes, and F. Blaabjerg, "Transformerless inverter topologies for single-phase photovoltaic systems: A comparative review," *IEEE J. Emerg. Sel. Topics Power Electron.*, vol. 8, no. 1, pp. 805–835, Mar. 2020, doi: 10.1109/JESTPE.2019.2908672.

[3] B. K. Santhoshi, K. M. Sundaram, S. Padmanaban, J. B. Holm-Nielsen, and K. K. Prabhakaran, "Critical review of PV grid-tied inverters," *Energies*, vol. 12, no. 10, pp. 1–26, 2019.

[4] M. Y. Ali Khan, H. Liu, Z. Yang, and X. Yuan, "A comprehensive review on grid connected photovoltaic inverters, their modulation techniques, and control strategies," *Energies*, vol. 13, no. 16, p. 4185, Aug. 2020.

[5] K. Zeb, W. Uddin, M. A. Khan, Z. Ali, M. U. Ali, N. Christofides, and H. J. Kim, "A comprehensive review on inverter topologies and control strategies for grid connected photovoltaic system," *Renew. Sustain. Energy Rev.*, vol. 94, pp. 1120–1141, Oct. 2018.

[6] H. Hu, S. Harb, N. Kutkut, I. Batarseh, and Z. J. Shen, "A review of power decoupling techniques for microinverters with three different decoupling capacitor locations in PV systems," *IEEE Trans. Power Electron.*, vol. 28, no. 6, pp. 2711–2726, Jun. 2013, doi: 10.1109/TPEL.2012.2221482.

[7] P. T. Krein, R. S. Balog, and M. Mirjafari, "Minimum energy and capacitance requirements for single-phase inverters and rectifiers using a ripple port," *IEEE Trans. Power Electron.*, vol. 27, no. 11, pp. 4690–4698, Nov. 2012, doi: 10.1109/TPEL.2012.2186640.

[8] A. R. Gautam, D. M. Fulwani, R. R. Makineni, A. K. Rathore, and D. Singh, "Control strategies and power decoupling topologies to mitigate 2ω-ripple in single-phase inverters: A review and open challenges," *IEEE Access*, vol. 8, pp. 147533–147559, 2020, doi: 10.1109/ACCESS.2020.3015315.

[9] L. Zhang, X. Ruan, and X. Ren, "Second-harmonic current reduction and dynamic performance improvement in the two-stage inverters: An output impedance perspective," *IEEE Trans. Ind. Electron.*, vol. 62, no. 1, pp. 394–404, Jan. 2015, doi: 10.1109/TIE.2014.2331015.

[10] M. Y. A. Khan, H. Liu, S. Habib, D. Khan, and X. Yuan, "Design and performance evaluation of a step-up DC–DC converter with dual loop controllers for two stages grid connected PV inverter," *Sustainability*, vol. 14, no. 2, p. 811, Jan. 2022, doi: 10.3390/su14020811.

[11] G. C. Christidis, A. C. Kyritsis, N. P. Papanikolaou, and E. C. Tatakis, "Investigation of parallel active Filters' limitations for power decoupling on single-stage/single-phase microinverters," *IEEE J. Emerg. Sel. Topics Power Electron.*, vol. 4, no. 3, pp. 1096–1106, Sep. 2016, doi: 10.1109/JESTPE.2016.2552980.

[12] H. Watanabe, T. Sakuraba, K. Furukawa, K. Kusaka, and J.-I. Itoh, "Development of DC to single-phase AC voltage source inverter with active power decoupling based on flying capacitor DC/DC converter," *IEEE Trans. Power Electron.*, vol. 33, no. 6, pp. 4992–5004, Jun. 2018, doi: 10.1109/TPEL.2017.2727063.

[13] S. Bhowmick and L. Umanand, "Design and analysis of the low device stress active power decoupling for single-phase grid connection for a wide range of power factor," *IEEE J. Emerg. Sel. Topics Power Electron.*, vol. 6, no. 4, pp. 1921–1931, Dec. 2018, doi: 10.1109/JESTPE.2018.2794784.

[14] Y.-C. Chen, L.-R. Chen, C.-M. Lai, Y.-C. Lin, and T.-J. Kuo, "Development of a DC-side direct current controlled active ripple filter for eliminating the double-line-frequency current ripple in a single-phase DC/AC conversion system," *Energies*, vol. 13, no. 18, p. 4772, Sep. 2020, doi: 10.3390/en13184772.

[15] Z. Yang, J. Zeng, Q. Zhang, Z. Zhang, V. Winstead, and D. Yu, "A composite power decoupling method for a PV inverter with optimized energy buffer," *IEEE Trans. Ind. Appl.*, vol. 57, no. 4, pp. 3877–3887, Jul. 2021, doi: 10.1109/TIA.2021.3079162.

[16] E. Rikos, S. Tselepis, C. Hoyer-Klick, and M. Schroedter-Homscheidt, "Stability and power quality issues in microgrids under weather disturbances," *IEEE J. Sel. Topics Appl. Earth Observ. Remote Sens.*, vol. 1, no. 3, pp. 170–179, Sep. 2008, doi: 10.1109/JSTARS.2008.2010557.

[17] R. Tonkoski, L. A. C. Lopes, and T. H. M. El-Fouly, "Coordinated active power curtailment of grid connected PV inverters for overvoltage prevention," *IEEE Trans. Sustain. Energy*, vol. 2, no. 2, pp. 139–147, Apr. 2011, doi: 10.1109/TSTE.2010.2098483.

[18] M. Savaghebi, A. Jalilian, J. C. Vasquez, and J. M. Guerrero, "Autonomous voltage unbalance compensation in an islanded droop-controlled microgrid," *IEEE Trans. Ind. Electron.*, vol. 60, no. 4, pp. 1390–1402, Apr. 2013, doi: 10.1109/TIE.2012.2185914.
[19] S. G. Varzaneh, A. Raziabadi, M. Hosseinzadeh, and M. J. Sanjari, "Optimal energy management for PV-integrated residential systems including energy storage system," *IET Renew. Power Gener.*, vol. 15, no. 1, pp. 17–29, Jan. 2021.
[20] A. A. A. El-Ela, R. A. El-Seheimy, A. M. Shaheen, W. A. Wahbi, and M. T. Mouwafi, "PV and battery energy storage integration in distribution networks using equilibrium algorithm," *J. Energy Storage*, vol. 42, Oct. 2021, Art. no. 103041, doi: 10.1016/j.est.2021.103041.
[21] S. J. Hossain, B. D. Biswas, R. Bhattarai, M. Ahmed, S. Abdelrazek, and S. Kamalasadan, "Operational value-based energy storage management for photovoltaic (PV) integrated active power distribution systems," *IEEE Trans. Ind. Appl.*, vol. 55, no. 5, pp. 5320–5330, Sep. 2019, doi: 10.1109/TIA.2019.2920229.
[22] Y. Huo and G. Gruosso, "A novel ramp-rate control of grid-tied PV-battery systems to reduce required battery capacity," *Energy*, vol. 210, Nov. 2020, Art. no. 118433.

LIANG-RUI CHEN (Member, IEEE) was born in Changhua, Taiwan, in 1971. He received the B.S., M.S., and Ph.D. degrees in electronic engineering from the National Taiwan University of Science and Technology, Taipei, Taiwan, in 1994, 1996, and 2001, respectively. He joined as a Faculty Member with the Department of Eletrical Engineering, National Changhua University of Education, Changhua, in August 2006, where he is currently a Professor. His major research interests include power electronics, battery charging/balancing systems, and automatic control.

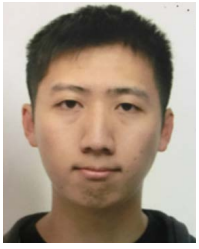

CHIA-HSUAN WU was born in Taipei, Taiwan, in 1985. He received the B.S., M.S., and Ph.D. degrees in electronic engineering from the National Chunghwa University of Education, Chunghwa, Taiwan, in 2008, 2010, and 2016, respectively. His major research interests include DC–AC power convertors, renewable energy, and battery charger.

NENG-YI CHU was born in Taoyuan, Taiwan, in 1984. He received the Ph.D. degree in electronic engineering from the National Taiwan University of Science and Technology, Taipei, Taiwan. He joined as a Faculty Member with the National Penghu University of Sicence and Technology, Penghu, in 2021, where he is currently an Assistant Professor. His research interests include microcontroller control, bidirectional converter design, fluorescent-lamp electronic ballasts, and control applications.

CHENG-CHIH CHOU was born in Kaohsiung, Taiwan, in 1982. He received the M.S. degree from the Institute of Ocean Technology and Marine Affairs (IOTMA), National Cheng Kung University (NCKU), Tainan, Taiwan, in 2008. He is currently pursuing the Ph.D. degree with Department of Electrical Engineering, National Changhua University of Education, Changhua, Taiwan.

He joined as a Faculty Member with the Green Energy and Environment Research Laboratories, Industrial Technology Research Institute, Hsinchu, in 2010, where he is currently an Senior Administrator. His research interests include renewable energy policy, green electrical market, T-REC, renewable portfolio standard.

FAN-JUN ZHENG was born in Taichung, Taiwan, in 1989. He received the B.S. and M.S. degrees in electrical engineering from the National Changhua University of Education, Changhua, Taiwan, in 2009 and 2011, respectively. Since 2019, he has been a Research Engineer with P-DUKE Technology Company Ltd.